Advanced Composites and Hybrid Materials (2022) 5:2031–2041
https://doi.org/10.1007/s42114-022-00547-7

ORIGINAL RESEARCH

Carboxyl-functionalized poly(arylene ether nitrile)-based rare earth coordination polymer nanofibrous membrane for highly sensitive and selective sensing of Fe^{3+} ions

Hang Yin[1,2] · Wanting Zhong[1] · Mao Yin[1] · Changjiang Kang[1] · Lulin Shi[1] · Hailong Tang[1,3] · Chaolong Yang[1] · Jalal T. Althakafy[4] · Mina Huang[5] · Abdullah K. Alanazi[6] · Lunjun Qu[1] · Youbing Li[1]

Received: 28 May 2022 / Revised: 12 July 2022 / Accepted: 17 August 2022 / Published online: 2 September 2022

Abstract

As a virtually indispensable metal ion for biological environments and human life, deficiency or accumulation of Fe^{3+} in the body can induce various biological disorders. It is of great significance to develop a rapid, reproducible, highly sensitive, and selective method for detecting Fe^{3+} ions. Herein, a kind of novel nanofibrous membrane prepared by electrospinning utilizing carboxyl-functionalized poly(arylene ether nitrile) (CPEN) as carrier of lanthanide sensor can serve as a simple and reliable fluorescence platform for identifying Fe^{3+} ions. The CPEN-Eu^{3+}-Phen nanofibrous membrane emitted intense red fluorescence under UV irradiation with high quantum efficiency of 22.3%. Furthermore, CPEN-Eu^{3+}-Phen exhibited excellent fluorescence stability under the NaCl concentrations of 0–1.0 M and pH of 1–14, ascribed to exceptional chemical durability of CPEN. Notably, the CPEN-Eu^{3+}-Phen implied excellent reusable performance for detecting Fe^{3+} ions with more than 10 cycles of reuse. Moreover, the red fluorescence of nanofibrous membrane is notably quenched with addition of Fe^{3+} ions, and the detection limit for Fe^{3+} in aqueous solution is as low as 3.8 μM. More importantly, CPEN-Eu^{3+}-Phen nanofibrous membrane can also be applied to the detection of Fe^{3+} ions in real lake water. In brief, these results indicated that CPEN-Eu^{3+}-Phen nanofibrous membrane is expected to behave as a promising Fe^{3+} ion sensing material with high selectivity, sensitivity, and reusability in aqueous solution.

Keywords Fe^{3+} ions detection · Nanofibrous membrane · Poly(arylene ether nitrile) · Fluorescence quenching · Fluorescent sensor

1 Introduction

A great diversity of inorganic/organic elements plays a crucial role in maintaining the balance of the biological system. Iron ions, as a virtually indispensable micronutrient for human and animal life, are authenticated to be involved in multiple fundamental physiological processes (e.g., cytochrome synthesis, enzymes formations, hematopoiesis, oxygen and nutrients transport, hemoglobin productions) [1–3]. Insufficient iron can induce the cellular anemia, metabolic disorder, and decrease of immunity capacity. Nevertheless, excessive iron ions in the human

✉ Hailong Tang
hailong.tang@cqut.edu.cn

1 School of Materials Science and Engineering, Chongqing University of Technology, Chongqing 400054, China

2 Key Laboratory for Organic Electronics and Information Displays & Institute of Advanced Materials, Jiangsu Key Laboratory for Biosensors, Jiangsu National Synergetic Innovation Center for Advanced Materials, Nanjing University of Posts and Telecommunications, Nanjing 210023, Jiangsu, China

3 Chongqing Shanwaishan Blood Purification Technology Co., Ltd, Chongqing 401123, China

4 Chemistry Department, Faculty of Applied Science, Umm Al-Qura University, Makkah, Saudi Arabia

5 College of Materials Science and Engineering, Taiyuan University of Science and Technology, Taiyuan 030024, Shanxi, China

6 Department of Chemistry, College of Science, Taif University, P.O. Box 11099, Taif 21944, Saudi Arabia

body may trigger hereditary hemochromatosis, thalassemia, etc. Additionally, iron is also a non-negligible ambient contaminant in industry [4–7]. Hence, it is of great significance to develop a portable, low-cost, sensitive approach for iron ion detection as to lessen environmental pollutions and protect human health.

Fluorescent sensors have been applied extensively in metal ion detection fields owing to its intrinsic superiorities such as remarkable sensitivity, simplicity, and ultrafast speed as compared with the traditional detection methods (e.g., X-ray diffractions, inductively coupled plasma mass spectrometry, atomic absorptions spectroscopy, atomic fluorescence spectrometry, and high-performance liquid chromatography), which are a relatively promising chemical detection technology [8–15]. Although many fluorescent sensors have been reported, they are usually disposable while measured. The sensors contaminated with analytes are often hard to clean, limiting greatly the large-scale applications. In this case, it is necessary to develop a fluorescent sensor with excellent reusability, selectivity, and sensitivity. With the advances in nanotechnology, nanocomposites are widely used in many fields such as microwave absorbers [16–18], dielectric materials [19, 20], and solar cells [21]. Electrospinning is considered to be a versatile and viable technology for electrostatic nanofiber formations with simple operations and low cost, and has been applied extensively in diverse fields, including filtrations and optical electronics, etc. [22, 23]. Fluorescent conjugated polymer nanofiber fabricated by electrospinning has been increasingly reported as optical chemosensors and biosensors [24–28]. The nanofiber sensors have excellent reversibility as well as fluorescence stability, which provide a distinguished alternative for achieving the repeatability of sensors with less loss of fluorescence intensity during the reuse. Furthermore, the nanofibrous membrane has an exceedingly high surface-to-volume ratio in virtue of irregular accumulations of nanofiber, which can significantly increase the sensitivity of metal ion detection.

As is well-known, poly(arylene ether nitrile) is an outstanding engineering plastic with excellent heat resistance, insulations, chemical resistance, and high mechanical strength in comparison with aliphatic polymers (e.g., poly(lactide-co-glycolide), poly(vinyl alcohol), poly (glycolide)) [29–35]. Herein, a novel carboxyl-functionalized poly(arylene ether nitrile) (CPEN) was used as macromolecular carrier of lanthanide sensors, which can not only avoid the small molecule probes falling off from polymer matrix due to strong covalent bonds, but also provide the possibility to detect iron ions under severe environment (e.g., strong acid, strong base) because of excellent chemical durability of CPEN [36]. Accordingly, a rational design to quickly and sensitively identify Fe^{3+} ions through fluorescence behavior by on–off switching of the sensor bonded to CPEN was exploited, which will offer a potential application for detecting iron ions with remarkable reusability (more than 10 cycles), high selectivity, and sensitivity (detection limit as low as 3.8 μM).

2 Experimental section

2.1 Materials

Phenolphthalin (PPL) and CPEN were synthesized according to a previously reported procedure in our laboratory [29], as also described in Experimental Section S1 in Supplementary Information. Rare earth chloride hexahydrate ($EuCl_3 \cdot 6H_2O$ and $TbCl_3 \cdot 6H_2O$), 1, 10-phenanthroline (Phen), $ZnCl_2$, KCl, $BaCl_2$, $FeCl_3$, $MgCl_2$, $MnCl_2$, $CuCl_2$, $FeCl_2 \cdot 4H_2O$, $HgCl_2$, $CoCl_2$, $NiCl_2 \cdot 6H_2O$, Pb $(NO_3)_2$, and $AgNO_3$ were obtained from Titan Scientific Co., Ltd., Shanghai, China. N, N-dimethylformamide (DMF) was acquired from Kelong Chemical Co., Ltd., Chengdu, China. DMF was dried and distilled under reduced pressure just before use. Ethylenediaminetetraacetic acid disodium salt (EDTA-2Na) was supplied by Hengxing Chemical Preparations Co., Ltd., Tianjin, China.

2.2 Fabrication of rare earth coordination polymer nanofibrous membranes

The schematic diagram of CPEN-Eu3 + xTb3 + 1-x-Phen (x = 0, 0.25, 0.5, 0.75, 1) coordination polymers is shown in Scheme 1. Firstly, CPEN solution was prepared by dissolving CPEN (1.10 g) into 5 ml DMF under stirring at 60 °C for 0.5 h. Next, the well-stirred compound solution of $RECl_3 \cdot 6H_2O$ (0.54 g of $EuCl_3 \cdot 6H_2O$ or 0.55 g of $TbCl_3 \cdot 6H_2O$) and Phen (0.58 g) in 5 mL DMF was poured into the as-prepared CPEN solution, and then stirred at 60 °C for 4 h to form a uniform rare earth coordination polymer solution with 200 mg/mL through solvent volatilizations. ^{1}H NMR of CPEN (400 MHz, DMSO-d6, ppm): δ = 1.7 (s, 6H, $2CH_3$), 6.59–7.84 (m, 26H, 26CH in benzene rings of polymer backbone), 6.71 (s, 1H, CH), 12.99 (s, 1H, COOH); ^{1}H NMR (400 MHz, DMSO-d6, ppm) of CPEN-Eu^{3+}-Phen: δ = 1.71 (s, 6H, $2CH_3$), 6.61–7.76 (m,26H, 26CH belong to benzene rings of polymer backbone), 6.73 (s, 1H, CH), 12.99 (s, 1H, COOH), 8.04–9.10 (m, 16H, 16CH belong to benzene rings of 1, 10-phenanthroline). FT-IR (KBr pellet, v/cm^{-1}) of Phen: 3063(w), 1647(w), 1616(w), 1588(w), 1559(w), 1504(s), 1421(s), 1344(w), 1215(w), 1139(w), 1092(w), 853(s), 737(s); FT-IR (KBr pellet, v/cm^{-1}) of CPEN: 2967(w), 2229 (w), 1725 (s), 1600 (w), 1575 (w), 1501(s), 1457(s), 1242(s), 1020(s); FT-IR (KBr pellet, v/cm^{-1}) of CPEN-Eu^{3+}: 2967(w), 2229

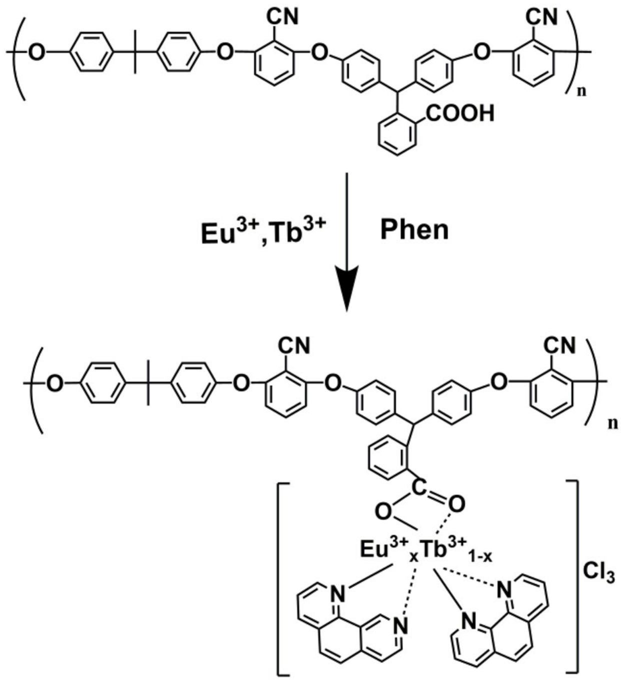

Scheme 1 Structural expressions of CPEN-Eu3 + xTb3 + 1-x-Phen (x = 0, 0.25, 0.5, 0.75, 1) coordination polymers

(w),1641(s), 1600(w),1577(w), 1501(s), 1459(s),1404(s), 1243(s), 1022(s); FT-IR (KBr pellet, v/cm^{-1}) of CPEN-Eu^{3+}-Phen: 2967(w), 2229(w), 1640(s), 1600(w), 1575(w), 1525(w), 1501(s), 1459(s), 1420(s), 1405(s), 1243(s), 1022(s), 846(s), 727(s). FT-IR (KBr pellet, v/cm^{-1}) of CPEN-Tb^{3+}-Phen: 2968(w), 2229(w), 1638(s), 1600(w), 1576 (w), 1522(w), 1501(s), 1459(s), 1421(s), 1400(s), 1243(s), 1022(s), 844(s), 725(s).

For the electrospinning process, the as-fabricated CPEN-Eu^{3+}-Phen solution was sucked into a syringe of 5 mL, which was extruded with the positive voltage of 18 kV at an injections speed of 0.1 mm/min. A stainless-steel needle with an inner diameter of 0.5 mm was used as the nozzle of the syringe across a distance of 16 cm between the needle tip and the collector. The temperature and relative humidity were kept at 30 °C and ~ 35%, respectively. A roller covered with a layer of 30-cm-wide silicon paper acted as the collector, which was connected to the negative electrode. The rare earth coordination polymer nanofibrous membranes were collected on silicone oil paper with a rotational speed of 10 rpm and collection time of 5 h. Since the surface of the silicon paper was smooth and compact, it can ameliorate the weakness that the nanofiber was difficult to peel off. After electrospinning, the as-prepared nanofibrous membranes were transferred to a vacuum oven at 80 °C (for 2 h) for removing the residual solvent.

2.3 Characterizations

Thermogravimetric analysis (TGA) and derivative thermogravimetric (DTG) analysis were recorded with a TGA-Q50 system (TA Instruments, New Castle, USA) heated from 30 to 700 °C at a heating rate of 20 °C·min^{-1} under a flowing nitrogen atmosphere. Differential scanning calorimetry (DSC) was determined with a DSC-Q20 analyzer (TA Instruments, New Castle, USA) at a heating rate of 10 °C·min^{-1} from 30 to 300 °C in a nitrogen atmosphere. Luminescence spectra and fluorescence decay curves were recorded on an FLS1000 fluorescence spectrometer (Edinburgh Instruments, Livingston, UK). The ultraviolet photoluminescence was observed with a WFH-204B analyzer (Jing Ke Instruments, Shanghai, China) under UV-light irradiation at 254 nm. Nanofiber was prepared by ET-2535H electrospinning equipment (Yongkang Leye, Beijing, China). The micromorphology of nanofiber was measured utilizing JSM-6460LV scanning electron microscopy (JEOL, Tokyo, Japan) at 15 kV, accompanied with energy dispersive spectroscopy (EDS) for analysis elements. The water contact angle (CA) was completed on a Theta Lite optical contact angle measuring system (Biolin Scientific, Gothenburg, Sweden). X-ray diffraction (XRD) pattern was determined with a PANalytical Empyrean Series 2 diffractometer (Malvern Panalytical, UK) using Cu Kα radiation in a scanning range of 5–60° (2θ). X-ray photoelectron spectroscopy (XPS) was conducted on a Thermo Kalpha photoelectron spectrometer (Thermo Scientific, Waltham, USA). Fourier transform infrared (FTIR) spectra on KBr pellets were investigated with a Thermo Nicolet iS5 spectrometer (Thermo Scientific, Waltham, USA) in the 600–4000 cm^{-1} region. The proton nuclear magnetic resonance (^1H NMR) spectra were determined with an Avance 400 spectrometer (Bruker, Switzerland) at 400 MHz. Ultraviolet–visible (UV–Vis) absorption spectra were recorded with a PE lambda 750S spectrometer (PerkinElmer, Waltham, USA).

3 Results and discussions

3.1 Fluorescence properties of coordination polymer nanofibrous membrane

Figure 1a illustrates the formation process of CPEN-Eu3 + xTb3 + 1-x-Phen nanofibrous membrane. The precursor solutions composed of CPEN and molecular probe Eu3 + xTb3 + 1-x-Phen (x = 0, 0.25, 0.5, 0.75, 1) was stretched and emitted under the action of electrostatic field. Figure 1b shows the emission spectra of CPEN-Eu3 + xTb3 + 1-x-Phen recorded using 320 nm as the excitation wavelength. The characteristic fluorescence

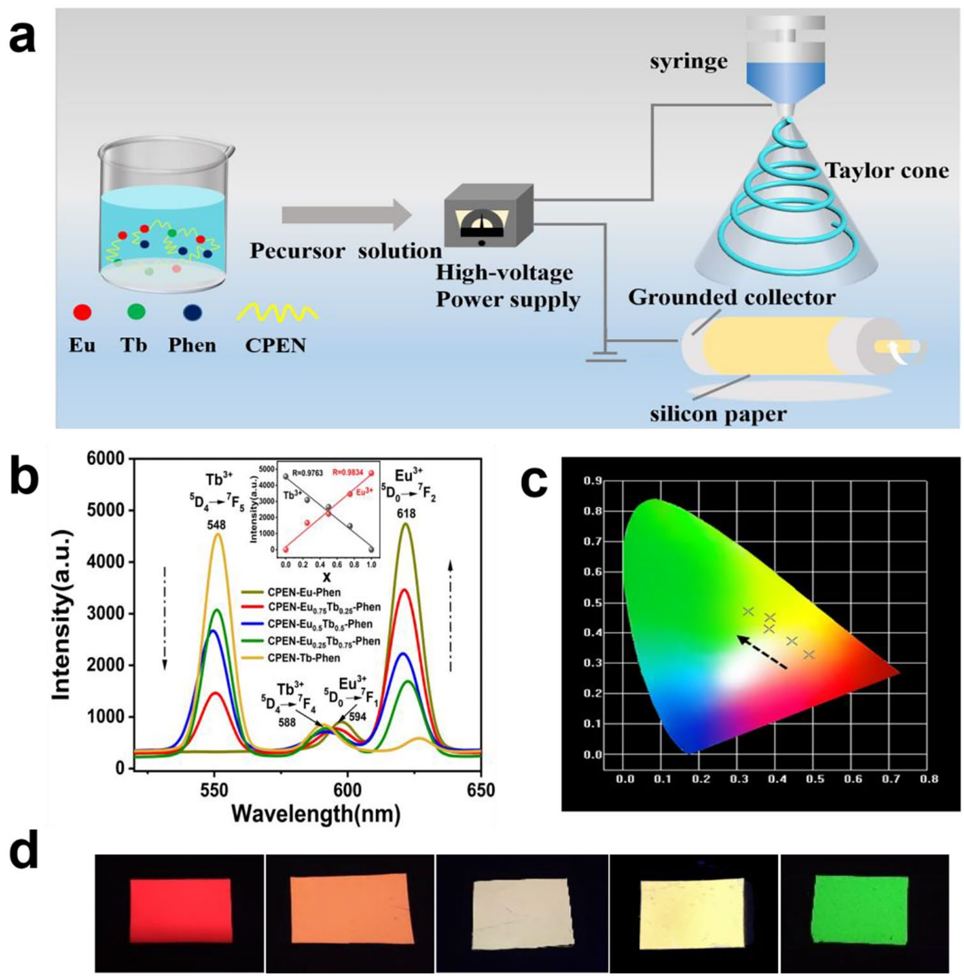

Fig. 1 **a** Schematic diagram of preparation of nanofibrous membranes. **b** Emission spectra of CPEN-Eu3 + *x*Tb3 + 1-x-Phen ($x = 0$, 0.25, 0.5, 0.75, 1) using 320 nm as the excitation wavelength. The insert shows the linear relationship between fluorescence intensity and ratio of Eu^{3+} (Tb^{3+}) at 618 (548) nm in the CPEN-Eu3 + xTb3 + 1-x-Phen system. **c** Trajectory of color modulations, recorded by the change of the ratio of Eu^{3+} and Tb^{3+} in the Commission Internationsale de L'Eclairage (CIE) coordinate diagram. **d** Photographs of the nanofibrous membranes taken under the UV light irradiation of 254 nm

emission peaks of CPEN-Eu3 + *x*Tb3 + 1-x-Phen are located at 618 nm ($D_0 \rightarrow {}^7F_2$ transitions of Eu^{3+}) and 548 nm (${}^5D_4 \rightarrow {}^7F_5$ transitions of Tb^{3+}), respectively. The emission intensity of Eu^{3+} increased with the increase of *x* values, yet emissions intensity of Tb^{3+} was just the opposite. Besides, the linear regression coefficients for Eu^{3+} and Tb^{3+} were 0.9834 and 0.9763, respectively. In order to reveal the mark of color variations, the trajectory of color modulations was intuitively depicted in the CIE coordinate diagram (Fig. 1c) by adjusting the concentrations of Eu^{3+} and Tb^{3+}. Taking CPEN-$Eu^{3+}{}_{0.75}Tb^{3+}{}_{0.25}$-Phen as an example, the (0.445, 0.373) regarded as a chromaticity coordinate falls into orange regions of the CIE coordinate diagram where the image of nanofiber exhibited orange fluorescence under UV light irradiations of 254 nm. As displayed in Fig. 1d, the various colors of CPEN-Eu3 + *x*Tb3 + 1-x-Phen changed from red to yellow, then to green. Meanwhile, EDS was employed to analyze chemical compositions concerning the content of Eu^{3+} and Tb^{3+} (Table S1 in Supplementary Inforation). The results demonstrated that the proportions of Eu^{3+} and Tb^{3+} ions in CPEN-Eu3 + *x*Tb3 + 1-x-Phen ($x = 0.25$, 0.5, 0.75) were very close to initial feed ratio, which further verified the fluorescence color of CPEN-Eu3 + *x*Tb3 + 1-x-Phen was associated with the ratio of Eu^{3+} and Tb^{3+}.

To further verify the structure of CPEN-Eu^{3+}-Phen, it was characterized by XPS and XRD, respectively. It is noteworthy that the peak of O 1 s was split into two peaks, where the component at 532.2 eV of CPEN was assigned to the ether bond and another at 533.5 eV was ascribed to the carbonyl group in carboxyl group (Fig. 2b) [37]. It can be seen that the O 1 s peak located at 533.5 eV from the carbonyl group of CPEN-Eu^{3+}-Phen shifted to 534 eV, demonstrating the appearance of bonding interactions between the O atom of CPEN and the Eu^{3+} ions. This was principally because the lone pair electrons of oxygen on the carboxyl group of CPEN-Eu^{3+}-Phen were partially transferred to the outer vacant orbitals of Eu^{3+} ions, which decreased the outer charge density of oxygen, thereby increasing binding energy for O 1 s. Meanwhile, the peak at 398.6 eV of Phen was attributed to the aromatic N, which from the aromatic N of CPEN-Eu^{3+}-Phen shifted to 399.3 eV, suggesting the existence of bonding interactions between the N atom of Phen and the Eu^{3+} ions. As shown in Fig. 2d, CPEN-Eu^{3+}-Phen

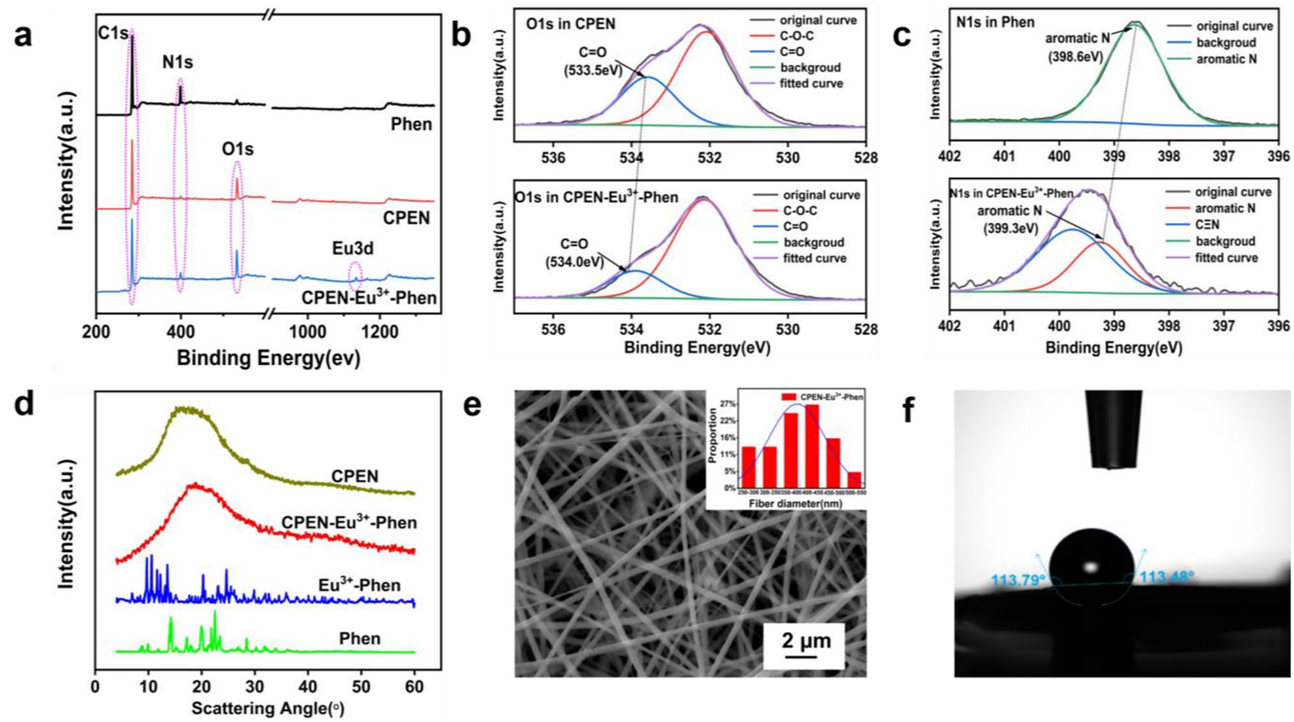

Fig. 2 **a** XPS full spectra of CPEN-Eu^{3+}-Phen, CPEN, and Phen. **b** XPS spectra for the O 1 s region of CPEN-Eu^{3+}-Phen and CPEN. **c** XPS spectra for the N 1 s region of CPEN-Eu^{3+}-Phen and CPEN. **d** XRD patterns of the CPEN-Eu^{3+}-Phen and CPEN, Eu^{3+}-Phen, and Phen (for comparison). **e** SEM image of CPEN-Eu^{3+}-Phen nanofibrous membrane. The insert shows the diameter distribution of the nanofibers. **f** Magnified photograph of water contact angle of CPEN-Eu^{3+}-Phen nanofibrous membrane

exhibited a diffuse peak similar to CPEN but opposite to the sharp crystalline peaks of Eu^{3+}-Phen and Phen, indicating that CPEN-Eu^{3+}-Phen showed an amorphous structure.

Additionally, the morphologies of nanofibrous membrane can be visually observed according to the electromicroscopy (Fig. 2e). Taking CPEN-Eu^{3+}-Phen as an example, it was found that the nanofiber was uniformly distributed and the surface was smooth. Besides, the size distribution of fiber diameter was acquired by employing Image-Pro Plus analysis, and the diameter distribution is mainly in the range of 350 − 450 nm (Insert in Fig. 2e). Furthermore, the contact angle (CA) of CPEN-Eu^{3+}-Phen is displayed in Fig. 2f, implying a water contact angle of $(113.6 \pm 0.2)°$. The nanofibrous membrane exhibited moderate hydrophobicity, which will increase repeatable stability of the sensors.

3.2 Thermal properties and fluorescence stabilities of coordination polymer nanofibrous membrane

As shown in Fig. 3a, the thermal stability of CPEN and CPEN-Eu3 + xTb3 + 1-x-Phen (x = 0, 0.25, 0.5, 0.75, 1) nanofibrous membrane was measured by TGA ranging from room temperature to 700 °C, and their derivative thermogravimetry (DTG) curves are also shown in Fig. S1 in Supplementary Information. It was noteworthy that all CPEN-Eu3 + xTb3 + 1-x-Phen had similar thermal decompositions process, presenting two thermal decompositions steps in comparison with only one mass loss step of CPEN ascribed to polymer skeleton decompositions. The first mass loss occurring from 210 to 450 °C was attributed to the degradations of coordination bonds and eliminations of Phen. The second mass loss was caused by the decompositions of polymer backbone which began at 500 °C. On the basis of the analysis, it further corroborated the probe molecule Eu3 + xTb3 + 1-x-Phen were successfully coordinated to CPEN, thus forming the CPEN-Eu3 + xTb3 + 1-x-Phen coordination polymers [38, 39]. As shown in Fig. 3b, the thermal properties of CPEN and CPEN-Eu3 + xTb3 + 1-x-Phen were investigated by DSC in the range of 30–300 °C. In comparison with the glass transitions temperature (T_g) of CPEN (195 °C), there was no obvious T_g for CPEN-Eu3 + xTb3 + 1-x-Phen. This is primarily because the presence of the multi-chelate rings formed by the rigid Phen and the polymer backbone around rare earth ions can increase steric hindrance in molecules, hence enhancing T_g beyond observations temperature range [40].

In order to evaluate the fluorescence stability of nanofibrous membranes under severe natural environment, as the case of CPEN-Eu^{3+}-Phen, the response of fluorescence intensity was

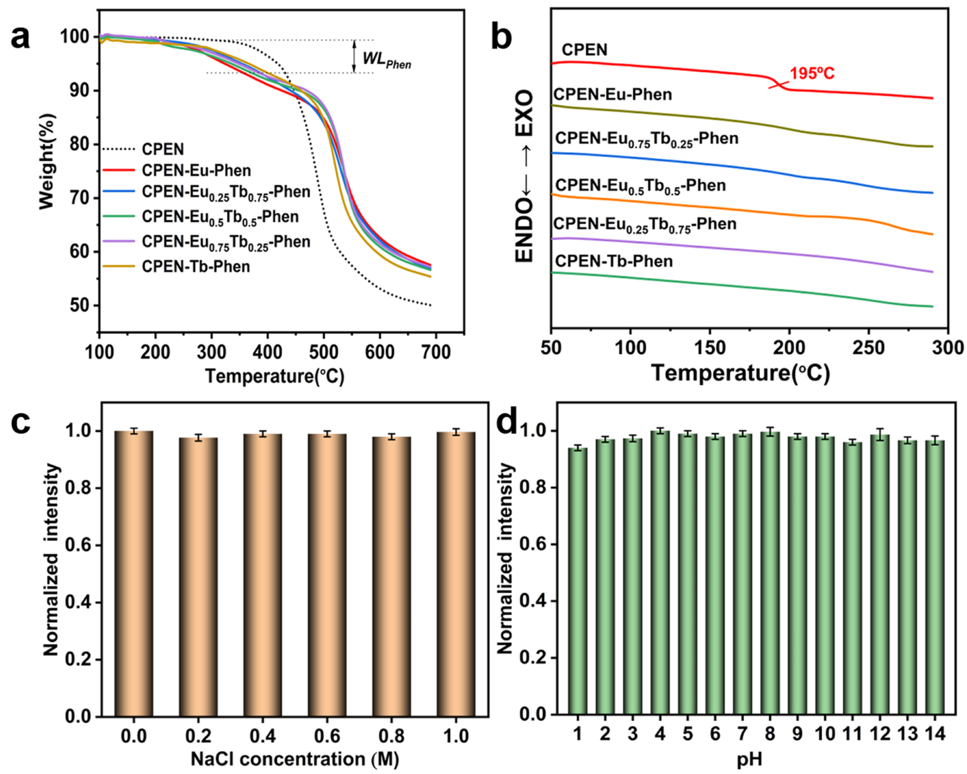

Fig. 3 **a** TGA and **b** DSC curves of CPEN and CPEN-Eu3 + *x*Tb3 + 1-x-Phen (*x* = 0, 0.25, 0.5, 0.75, 1). **c** Effect of NaCl concentrations on the normalized fluorescence intensity of CPEN-Eu^{3+}-Phen at 618 nm. **d** Effect of pH on the normalized fluorescence intensity of CPEN-Eu^{3+}-Phen at 618 nm

investigated thoroughly by simulating acid, alkali, and salt environment created by regulating pH and NaCl concentrations. It was clearly found that the normalized fluorescence intensity of CPEN-Eu^{3+}-Phen substantially unchanged at NaCl concentrations of 0–1.0 M and pH value ranging from 1 to 14 (Fig. 3c–d). Hence, CPEN-Eu^{3+}-Phen exhibited excellent fluorescence stability in an acid, alkali, and salt environment, which mainly originated from exceptional chemical durability of CPEN. In addition, in order to investigate comprehensively the photophysical properties of CPEN-Eu^{3+}-Phen, the fluorescence lifetime was 1.25 ms calculated by a double-exponential decay function. On the basis of the value of the fluorescence lifetime, the photoluminescence quantum efficiency of CPEN-Eu^{3+}-Phen was determined by the following equation [41]:

$$\eta = \frac{A_{rad}}{A_{rad} + A_{nrad}}$$

where η referred to the photoluminescence quantum efficiency, A_{rad} was the radiative transitions rate, and A_{nrad} was the non-radiative transitions rate. The total radiative transitions rate was obtained by the following formula ($A_{total} = A_{rad} + A_{nrad} = \tau^{-1}$, where τ referred to obtained fluorescence lifetime). The quantum efficiency of CPEN-Eu^{3+}-Phen was as high as 22.3%. In brief, CPEN-Eu^{3+}-Phen nanofibrous membrane can be used as a fluorescence sensor with excellent thermal properties, fluorescence stability, and high quantum efficiency.

3.3 The effect of metal ions on photophysical properties

In an effort to investigate the selectivity of different cations for CPEN-Eu^{3+}-Phen nanofibrous membrane in detail, CPEN-Eu^{3+}-Phen was immersed in the diverse metal ions solution (0.01 M of K^+, Ni^{2+}, Zn^{2+}, Co^{2+}, Ba^{2+}, Cu^{2+}, Mg^{2+}, Pb^{2+}, Hg^{2+}, Fe^{2+}, Ag^+, Mn^{2+}, Fe^{3+}) for 20 min, and then their value of relative intensity (I/I_0) was recorded. It was worth noting that only addition of Fe^{3+} can notably quench the fluorescence intensity. However, other ions slightly affected fluorescence intensity toward sensors based on response of differences in electron configurations and energy transfer [42]. Hence, CPEN-Eu^{3+}-Phen was expected to serve as a promising platform for Fe^{3+} ions detection. Figure 4b indicated the variations in fluorescence intensity as a function of the concentration of Fe^{3+} ions. The quenching effect progressively enhanced with the increasing concentration of Fe^{3+} ions. Fluorescence quenching by Fe^{3+} ions was assessed using a Stern–Volmer equations (Ksv) [43–45].

$$I0/I = 1 + KSVC \quad (1)$$

where I_0 and I were emission intensities in the absence and presence of Fe^{3+} ions. K_{SV} was the Stern–Volmer content. C referred to the molar concentrations of Fe^{3+}. The results showed that the quenched emissions intensity was positively correlated with the Fe^{3+} concentrations in the

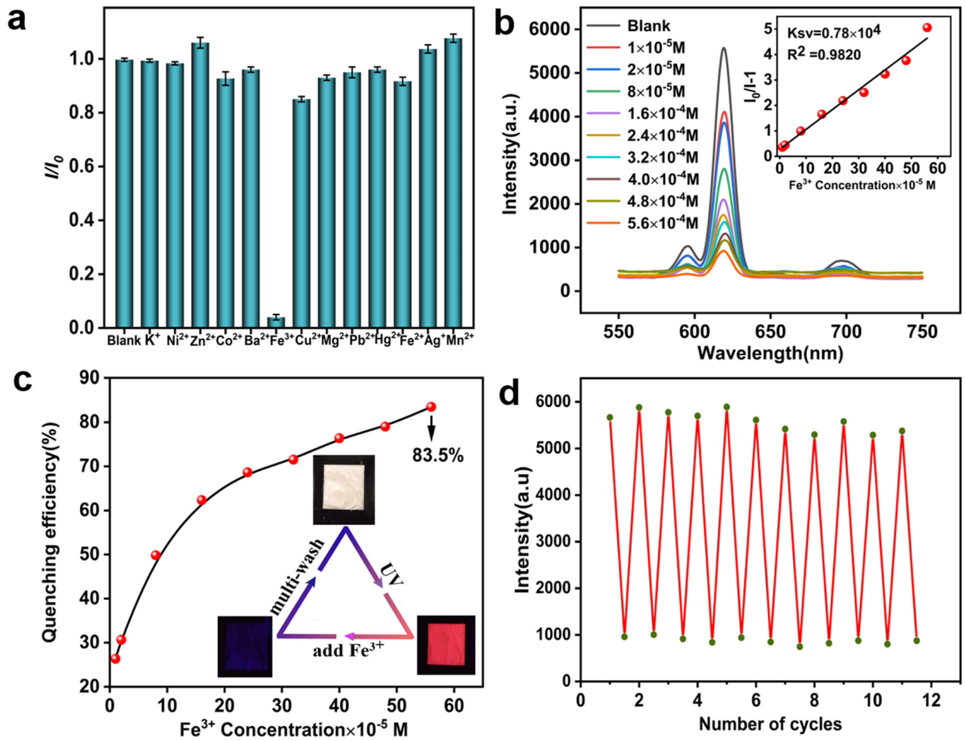

Fig. 4 **a** Comparison of fluorescence quenching effect of different cations (0.01 M of K^+, Ni^{2+}, Zn^{2+}, Co^{2+}, Ba^{2+}, Cu^{2+}, Mg^{2+}, Pb^{2+}, Hg^{2+}, Fe^{2+}, Ag^+, Mn^{2+}, Fe^{3+}) on CPEN-Eu^{3+}-Phen in aqueous solutions. **b** Effect of Fe^{3+} ion concentration on fluorescence intensity of CPEN-Eu^{3+}-Phen nanofibrous membrane ($\lambda_{ex}=320$ nm). The insert is Stern–Volmer calibrations curve for Fe^{3+} ions in aqueous solutions at pH = 7. **c** The variation tendency of fluorescence quenching efficiency with increase of Fe^{3+} ion concentrations in aqueous solutions ($\lambda_{ex}=320$ nm). The insert showed photographs of CPEN-Eu^{3+}-Phen under day light and 254-nm UV light irradiation in the presence and absence of Fe^{3+} ions. **d** Fluorescence intensity of CPEN-Eu^{3+}-Phen when multiple quenching and recovery

range of 1×10^{-5} to 5.6×10^{-4} M ($K_{sv}=0.78\times10^4$ M^{-1}). The limit of detections (LOD) for Fe^{3+} was determined to be 3.8 μM (LOD = $3\delta/S$, where δ is the standard deviation of 11 blank samples and S is the mean slope of the calibrations curve) with a regression coefficient, $R^2=0.9820$. When the concentration of Fe^{3+} ions reached the critical point (5.6×10^{-4} M) at which fluorescence quenching significantly occurred, the quenching efficiency of CPEN-Eu^{3+}-Phen reached 83.5% (Fig. 4c).

A comparison of different fluorescent sensing platforms with that obtained in present work is displayed in Table 1. Meanwhile, taking into account the practical sensing capability of real water system, the detection experiment of $FeCl_3$ lake water solution composed of the mixture of different concentration of Fe^{3+} stock solution and real lake water (from South Lake, Banan District, Chongqing, China) was investigated. The results revealed similar quenching effect as mentioned before, and S-V plot for Fe^{3+} ions showed good linearity between the emission intensity of CPEN-Eu^{3+}-Phen at 620 nm and the concentration of Fe^{3+} ions ($K_{sv}=0.62\times10^4$ M^{-1}, $R^2=0.9661$), demonstrating that the CPEN-Eu^{3+}-Phen had an efficient sensing performance for Fe^{3+} ions detection (Fig. S2 in Supplementary Information). Despite there may be many impurities (e.g., suspended solids or colloids) in the lake environment, the CPEN-Eu^{3+}-Phen was still effective for the detection of Fe^{3+} ions.

Considering the cost and reality of CPEN-Eu^{3+}-Phen sensing, the multiple quenching and recovery experiment was conducted. After being washed with EDTA-2Na (0.01 M) for five times in following each cycle, the fluorescence intensity of CPEN-Eu^{3+}-Phen was recovered again and can be recycled up to 11 times, as shown in Fig. 4d. This

Table 1 Comparison of different fluorescent sensing platforms for Fe^{3+} ion detection

Sensing platform for Fe^{3+}	LOD (μM)	Linear range (mM)	Ref
$[Eu_2(ppda)_2(npdc)(H_2O)]\cdot H_2O$	16.6	0–0.28	[37]
$[Eu(ctpy)(tta)_2]_n$ @PAN	668	0–4.80	[46]
SRhBOH/ poly (HEMA-co-NMA-co-NBD)	100	0.1–10	[47]
LaF_3: Ce,Tb nanoparticles	2.4	0.008–0.1	[48]
Anthracene-based Schiff base	2.9	0.002–0.06	[49]
$Eu_{0.24}Tb_{0.76}$-BHM-COOH	4.5	0–0.34	[5]
CPEN-Eu^{3+}-Phen	3.8	0–0.56	This work

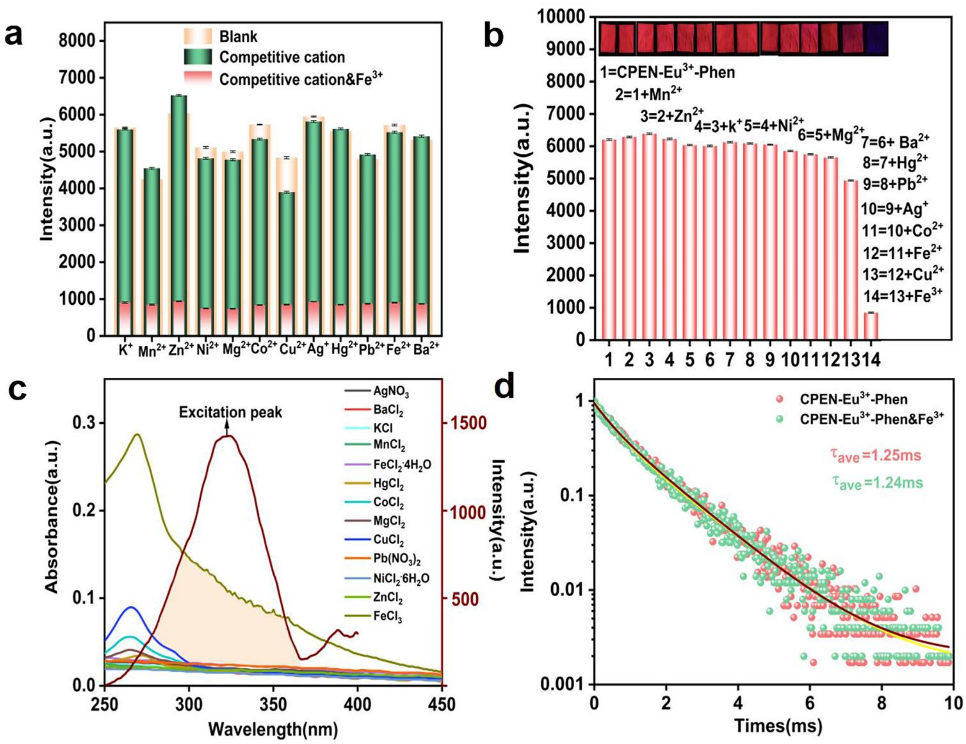

Fig. 5 **a** Competition experiment results of CPEN-Eu^{3+}-Phen for Fe^{3+} ion detection in the presence of different competitive cations (5.6×10^{-4} M). **b** Anti-interference experiment results of CPEN-Eu^{3+}-Phen for Fe^{3+} ion detection in the presence of multiple cations. The insert shows the luminescence photographs of samples 1–14 under 254-nm ultraviolet lamp. **c** UV–vis absorption spectra of different metal ions and excitation spectrum of CPEN-Eu^{3+}-Phen. **d** Fluorescence lifetime decay curves of CPEN-Eu^{3+}-Phen with and without addition of Fe^{3+} ions ($\lambda_{ex} = 320$ nm)

is probably because the nanofibrous membrane is moderately hydrophobic, which lead to easily removing Fe^{3+} ions from nanofiber surface.

As we all know, metal ions usually persisted in the environment together, rather than alone. Hence, it was essential to carry out competitions experiment for Fe^{3+} ion detection. As illustrated in Fig. 5a, the fluorescence intensity at 618 nm fluctuated slightly in comparison to original samples when dropping 5.6×10^{-4} M of other single competitive ions onto the surface of nanofibrous membrane, whereas the addition of Fe^{3+} ions can specifically quench the red fluorescence at 618 nm. Besides, the fluorescence intensity also changed slightly with the successive participations of multi-competitive ions (Fig. 5b). Until the addition of Fe^{3+} ions, the fluorescence quenching effect was pronounced. The above results showed that, whether these competitive ions exist individually or together, the detection of Fe^{3+} ions by CPEN-Eu^{3+}-Phen nanofibrous membrane was almost undisturbed. Furthermore, Fe^{3+} ions can be distinguished expediently among other ions by visually observing the quenching of red fluorescence, which was conducive to practical applications in the optical detection field. As a consequence, CPEN-Eu^{3+}-Phen nanofibrous membrane had high selectivity and anti-interference for Fe^{3+} ion detection.

To thoroughly explore the fluorescence quenching mechanism of CPEN-Eu^{3+}-Phen nanofibrous membrane, CPEN-Eu^{3+}-Phen was soaked in 0.01 M Fe^{3+} ions for 20 min, and then EDS was applied to identify whether the fluorescence quenching was caused by the ion exchange between Fe^{3+} ions and Eu^{3+} ions [37]. As shown in Table S2 in Supplementary Information, the content of Eu (11.90 wt%) is much higher than that of Fe (0.26 wt%), thus indicating negligible degree of cation exchange between Eu^{3+} and Fe^{3+} ions. Furthermore, UV–vis absorption spectra of different metal ions at the same concentration of 10^{-5} M were measured, as shown in Fig. 5c. By comparison, it was noticeable that the overlapping area between the UV–vis absorption spectrum of Fe^{3+} ions and the excitation spectrum of CPEN-Eu^{3+}-Phen is maximum. It means that, partial radiation energy derived from excitation light can be effectively absorbed by Fe^{3+} ions, which hindered efficient energy transfer from the ligands (i.e., CPEN and Phen) to luminescence center (i.e., Eu^{3+}), thereby resulting in a significant reduction of emission intensity. Namely, Fe^{3+} ions as a high efficiency quencher played a shielding role in the luminescence process. Therefore, the energy transfer caused by competitive absorptions between CPEN-Eu^{3+}-Phen and Fe^{3+} ions is the main cause of fluorescence quenching [5, 50]. Additionally, by comparing the UV–vis and FTIR spectra of CPEN-Eu^{3+}-Phen nanofibrous membrane before and after adding Fe^{3+} ions, it was found that there was no new peak or peak shift (Fig. S3 in Supplementary Information). Therefore, it can be eliminated that the fluorescence quenching is caused by the formation of non-luminescent intermediate by chemical reactions.

Actually, the quenching was a process that competes with the luminescence process to shorten the lifetime of the excited state of luminescent molecule. The quenching process may occur in the interactions between the quenching agent and the excited or ground states of a fluorophore. The former is called dynamic quenching and the latter is called static quenching. In the process of dynamic quenching, the excited state molecules lose their excitation energy and return to the ground state through the mechanism of energy transfer and charge transfer by colliding with the quenching agent [51]. Thus, the dynamic quenching efficiency is related to the lifetime of excited state molecules. As shown in Fig. 5d the fluorescence lifetime of CPEN-Eu^{3+}-Phen nanofibrous membrane is almost unchanged with the addition of Fe^{3+} ions, which can exclude the cause of dynamic quenching, implying that the fluorescence quenching process belongs to static quenching.

4 Conclusions

In summary, a fluorescence sensing nanofibrous membrane for rapidly detecting Fe^{3+} ions in aqueous solutions was successfully developed by utilizing CPEN as carrier of Eu^{3+}-Phen via electrospinning. The fluorescence properties of CPEN-Eu^{3+}-Phen nanofibrous membrane was almost unaffected by acid, alkali, and salt environment benefiting by the excellent chemical durability of CPEN. Moreover, the CPEN-Eu^{3+}-Phen nanofibrous membrane demonstrates low limit of detections (as low as 3.8 μM), high selectivity, and excellent anti-interference performance for Fe^{3+} ion detection. More importantly, the nanofibrous membrane can be reused for more than 10 times in aqueous solutions with less loss of fluorescence intensity, profiting from its surface hydrophobicity. Therefore, the CPEN-Eu^{3+}-Phen nanofibrous membrane is expected to serve as a distinguished luminescent sensor for Fe^{3+} ion detection in aqueous solutions and also serve as sensors or platform for other applications [52, 53].

Supplementary Information The online version contains supplementary material available at https://doi.org/10.1007/s42114-022-00547-7.

Funding This work was financially supported by the National Natural Science Foundations of China (No. 51603027), Project of Science and Technology Research Program of Chongqing Educations Commissions of China (No. KJZD-M201901101), Innovations Research Group at Institutions of Higher Educations in Chongqing (No. CXQT 19027), the Special Key Project of Technology Innovation and Application Development of Chongqing (No. cstc2020jscx-dxwtBx0025), and Graduate Student Innovation Program of Chongqing University of Technology (Nos. gzlcx20223003, gzlcx20223026, and gzlcx20223027). Althakafy J. T. would like to thank the Deanship of Scientific Research at Umm Al-Qura University for supporting this work (No. 22UQU4281758DSR05).

Declarations

Competing interests The authors declare no competing interests.

References

1. Gao X, Lu Y, He S, Li X, Chen W (2015) Colorimetric detection of iron ions (III) based on the highly sensitive plasmonic response of the N-acetyl-L-cysteine-stabilized silver nanoparticles. Anal Chim Acta 879:118–125
2. Wang L, Zhu H, Xu G, Hou X, He H, Wang S (2020) A biocompatible cellulose-nanofiber-based multifunctional material for Fe^{3+} detection and drug delivery. J Mater Chem C 8:11796–11804
3. Fan Q, Li J, Wang J, Yang Z, Shen T, Guo Y, Wang L, Irshad M, Mei T, Wang X (2020) Ultrasensitive Fe^{3+} ion detection based on carbon quantum dot-functionalized solution-gated graphene transistors. J Mater Chem C 8:4685–4689
4. Zhang Q, Wang J, Kirillov A, Dou W, Xu C, Xu C, Yang L, Fang R, Liu W (2018) Multifunctional Ln-MOF luminescent probe for efficient sensing of Fe(3+), Ce(3+), and acetone. ACS Appl Mater Interfaces 10:23976–23986
5. Jia P, Wang Z, Zhang Y, Zhang D, Gao W, Su Y, Li Y, Yang C (2020) Selective sensing of Fe(3+) ions in aqueous solution by a biodegradable platform based lanthanide metal organic framework. Spectrochim Acta Part A: Mol Biomol Spectro 230:118084
6. Tian J, Liu Q, Asiri A, Sun X, He Y (2015) Ultrathin graphitic C_3N_4 nanofibers: hydrolysis-driven top-down rapid synthesis and application as a novel fluorosensor for rapid, sensitive, and selective detection of Fe^{3+}. Sens Actuators B: Chem 216:453–460
7. Wang B, Hai J, Liu Z, Wang Q, Yang Z, Sun S (2010) Selective detection of iron(III) by rhodamine-modified Fe_3O_4 nanoparticles. Angew Chem Int Ed 49:4576–4579
8. Xue W, Zhang Y, Duan J, Liu D, Ma Y, Shi N, Chen S, Xie L, Qian Y, Huang W (2015) A highly sensitive fluorescent sensor based on small molecules doped in electrospun nanofibers: detection of explosives as well as color modulation. J Mater Chem C 3:8193–8199
9. Su Y, Zhang D, Jia P, Gao W, Li Y, Bai Z, Liu X, Deng Q, Xu J, Yang C (2019) Highly selective and sensitive long fluorescence lifetime polyurethane foam sensor based on Tb-complex as chromophore for the detection of H_2PO_4(-) in water. Spectrochim Acta Part A: Mol Biomol Spectro 217:86–92
10. Wu Z, Fu Z, Velasco E, Xing K, Wang H, Zou G, Huang X, Li J (2020) A robust and multifunctional calcium coordination polymer as a selective fluorescent sensor for acetone and iron(+3) and as a tunable proton conductor. J Mater Chem C 8:16784–16789
11. Guan L, Jiang Z, Cui Y, Yang Y, Yang D, Qian G (2021) An MOF-based luminescent sensor array for pattern recognition and quantification of metal ions. Adv Opt Mater 9:2002180
12. Si Y, Wang X, Li Y, Chen K, Wang J, Yu J, Wang H, Ding B (2014) Optimized colorimetric sensor strip for mercury(ii) assay using hierarchical nanostructured conjugated polymers. J Mater Chem A 2:645–652
13. Zhou JM, Shi W, Xu N, Cheng P (2013) Highly selective luminescent sensing of fluoride and organic small-molecule pollutants based on novel lanthanide metal-organic frameworks. Inorg Chem 52:8082–8090
14. Yue D, Wang Y, Chen D, Wang Z (2020) Solvent triggering structural changes for two terbium-based metal-organic frameworks and their photoluminescence sensing. Chem Commun 56:4320–4323
15. Jia K, Ji Y, He X, Xie J, Wang P, Liu X (2022) One-step fabrication of dual functional Tb(3+) coordinated polymeric micro/nano-structures for Cr (VI) adsorption and detection. J Hazard Mater 423:127166
16. Wu N, Zhao B, Chen X, Hou C, Huang M, Alhadhrami A, Mersal G, Ibrahim M, Tian J (2022) Dielectric properties and electromagnetic simulation of molybdenum disulfide and ferric oxide modified Ti_3C_2TX MXene hetero-structure for potential microwave

absorption. Adv Compos Hybrid Mater: https://doi.org/10.1007/s42114-022-00507-1
17. Xie P, Shi Z, Feng M, Sun K, Liu Y, Yan K, Liu C, Moussa T, Huang M, Meng S, Liang G, Hou H, Fan R, Guo Z (2022) Recent advances in radio-frequency negative dielectric metamaterials by designing heterogeneous composites. Adv Compos Hybrid Mater: https://doi.org/10.1007/s42114-022-00479-2
18. Gao T, Rong H, Mahmoud K, Ruan J, Ei-Bahy S, Faheim A, Li Y, Huang M, Nassan M, Zhao R (2022) Iron/silicon carbide composites with tunable high-frequency magnetic and dielectric properties for potential electromagnetic wave absorption. Adv Compos Hybrid Mater: https://doi.org/10.1007/s42114-022-00507-1
19. Zhang Z, Liu M, Ibrahim M, Wu H, Wu Y, Li Y, Mersal G, El-Azab I, El-Bahy S, Huang M, Jiang Y, Liang G, Xie P, Liu C (2022) Flexible polystyrene/graphene composites with epsilon-near-zero properties. Adv Compos Hybrid Mater: https://doi.org/10.1007/s42114-022-00486-3
20. Gao S, Zhao X, Fu Q, Zhang T, Zhu J, Hou F, Ni J, Zhu C, Li T, Wang Y (2022) Highly transmitted silver nanowires-SWCNTs conductive flexible film by nested density structure and aluminum-doped zinc oxide capping layer for flexible amorphous silicon solar cells. J Mater Sci Technol 126:152–160
21. Ma R, Cui B, Hu D, El-Bahy S, Wang Y, El Azab I, Elnaggar A, Gu H, Mersal G, Huang M, Murugadoss V (2022) Enhanced energy storage of lead-free mixed oxide core double-shell barium strontium zirconate titanate@magnesium aluminate@zinc oxide-boron trioxide-silica ceramic nanocomposites. Adv Compos Hybrid Mater. https://doi.org/10.1007/s42114-022-00509-z
22. Liu H, Wang H, Lu X, Murugadoss V, Huang M, Yang H, Wan F, Yu D, Guo Z (2022) Electrospun structural nanohybrids combining three composites for fast helicide delivery. Adv Compos Hybrid Mater, in press,. https://doi.org/10.1007/s42114-022-00478-3
23. Pan D, Yang G, Abo-Dief H, Dong J, Su F, Liu C, Li Y, Xu B, Murugadoss V, Naik N, El-Bahy S, El-Bahy Z, Huang M, Guo Z (2022) Vertically aligned silicon carbide nanowires/boron nitride cellulose aerogel networks enhanced thermal conductivity and electromagnetic absorbing of epoxy composites. Nano-Micro Lett 14:118–136
24. Bhardwaj N, Kundu S (2010) Electrospinning: a fascinating fiber fabrication technique. Biotechnol Adv 28:325–347
25. Long Y, Chen H, Yang Y, Wang H, Yang Y, Li N, Li K, Pei J, Liu F (2009) Electrospun nanofibrous film doped with a conjugated polymer for DNT fluorescence sensor. Macromol 42:6501–6509
26. Wang P, Zhao L, Shou H, Wang J, Zheng P, Jia K, Liu X (2016) Dual-emitting fluorescent chemosensor based on resonance energy transfer from poly (arylene ether nitrile) to gold nanoclusters for mercury detection. Sens Actuators B: Chem 230:337–344
27. Ghosh K, Saha S, Wang Z (2014) Ultra-sensitive detection of explosives in solution and film as well as the development of thicker film effectiveness by tetraphenylethene moiety in AIE active fluorescent conjugated polymer. Polym Chem 5:5638–5643
28. Jia K, Bai Y, Wang L, Luo Y, Hu W, He X, Wang P, Marks R, Liu X (2021) Emulsion confinement self-assembly regulated lanthanide coordinating polymeric microparticles for multicolor fluorescent nanofibers. Polym 230:124043
29. Yin H, Tang Z, Fu G, Ai X, Xia J, Tang H, Yang C, Qu L, Li Y (2020) Novel rare earth coordination polymers with greatly enhanced fluorescence by synergistic effect of carboxyl-functionalized poly (arylene ether nitrile) and 1,10-phenanthroline. Eur Polym J 141:110078
30. Tang H, Pu Z, Huang X, Wei J, Liu X, Lin Z (2014) Novel blue-emitting carboxyl-functionalized poly (arylene ether nitrile)s with excellent thermal and mechanical properties. Polym Chem 5:3673–3679
31. Tang H, Wang P, Zheng P, Liu X (2016) Core-shell structured $BaTiO_3$@polymer hybrid nanofiller for poly (arylene ether nitrile) nanocomposites with enhanced dielectric properties and high thermal stability. Compos Sci Technol 123:134–142
32. Guan X, Li H, Ma Y, Xue M, Fang Q, Yan Y, Valtchev V, Qiu S (2019) Chemically stable polyarylether-based covalent organic frameworks. Nat Chem 11:587–594
33. Hu H, Dong T, Sui Y, Li N, Ueda M, Wang L, Zhang X (2018) Correction: a thermally crosslinked multiblock sulfonated poly (arylene ether ketone nitrile) copolymer with a 1,2,3-triazole pendant for proton conducting membranes. J Mater Chem A 6:12162–12162
34. Feng M, Li C, He M, Huang Y, Luo J (2020) Poly (arylene ether nitrile) ternary dielectric composites modulated via polydopamine-assisted $BaTiO_3$ decorating MoS_2 sheets. Ceram Int 46:19181–19190
35. Wang P, Song T, Abo-Dief H, Song J, Alanazi A, Fan B, Huang M, Lin Z, Altalhi A, Gao S, Yang L, Liu J, Feng S, Cao T (2022) Effect of carbon nanotubes on the interface evolution and dielectric properties of polylactic acid/ethylene–vinyl acetate copolymer nanocomposites. Adv Compos Hybrid Mater 1–11
36. Heng L, Wang X, Dong Y, Zhai J, Tang B, Wei T, Jiang L (2008) Bio-inspired fabrication of lotus leaf like membranes as fluorescent sensing materials. Chem-An Asian J 3:1041–1045
37. Zhan Z, Liang X, Zhang X, Jia Y, Hu M (2019) A water-stable europium-MOF as a multifunctional luminescent sensor for some trivalent metal ions (Fe(3+), Cr(3+), Al(3+)), PO_4(3-) ions, and nitroaromatic explosives. Dalton Trans 48:1786–1794
38. Liu D, Shi Q, Wang Z (2012) Color-tunable heat-resistant polyaryletherketones co-coordinated with various rare earth ions. Opt Mater 34:1815–1821
39. Liu D, Yu H, Wang Z, Nie Q (2010) Synthesis and fluorescence properties of novel 1, 10-phenanthroline-functionalized polyaryletherketone and its rare earth complexes. Polym Int 59:937–944
40. Wang H, Tang H, Yang J, Li Y (2018) Synthesis of poly (arylene ether nitrile) and carboxyl-functionalized poly (arylene ether nitrile) with high thermal stability and their thermal decomposition kinetics. High Perform Polym 31:743–752
41. Ramos T, Berton G, Cassol T, Junior S (2018) Carboxyl-functionalized ionic liquids: synthesis, characterization and synergy with rare-earth ions. J Mater Chem C 6:6270–6279
42. Liu Y, Wang Z, Qin W, Hu Q, Tang B (2017) Fluorescent detection of Cu (II) by chitosan-based AIE bioconjugate. Chin J Polym Sci 35:365–371
43. Idrees M, Salam A (2021) Pyrene interaction with selected amines in aqueous sodium dodecyl sulphate (SDS). J Fluoresc 31:595–598
44. Su Y, Zhang D, Jia P, Gao W, Li Y, He J, Wang C, Zheng X, Yang Q, Yang C (2019) Bonded-luminescent foam based on europium complexes as a reversible copper (II) ions sensor in pure water. Eur Polym J 112:461–465
45. Su Y, Yu J, Li Y, Phua S, Liu G, Lim W, Yang X, Ganguly R, Dang C, Yang C (2018) Versatile bimetallic lanthanide metal-organic frameworks for tunable emission and efficient fluorescence sensing. Commun Chem 1:1–13
46. Bai C, Yan L, Hu H, Zou F, Zhang T, Xue G (2021) Electrospinning fabrication of europium-chain@polymer nanofiber films for visual detection of the Fe^{3+} ion. ACS Appl Polym Mater 3:4504–4511
47. Chen B, Kuo C, Huang Y, Lu S, Liang F, Jiang D (2015) Novel highly selective and reversible chemosensors based on dual-ratiometric fluorescent electrospun nanofibers with pH and Fe(3+)-modulated multicolor fluorescence emission. ACS Appl Mater Interfaces 7:2797–2808
48. Mi C, Wang T, Zeng P, Zhao S, Wang N, Xu S (2013) Determination of ascorbic acid via luminescence quenching of LaF_3: Ce, Tb nanoparticles synthesized through a microwave-assisted solvothermal method. Anal Methods 5:1463–1468
49. Shellaiah M, Wu Y, Singh A, Ramakrishnam Raju M, Lin H (2013) Novel pyrene- and anthracene-based schiff base derivatives as $Cu^{2+}$and Fe^{3+}fluorescence turn-on sensors and for aggregation induced emissions. J Mater Chem A 1:1310–1318

50. Wang L, Fan G, Xu X, Chen D, Wang L, Shi W, Cheng P (2017) Detection of polychlorinated benzenes (persistent organic pollutants) by a luminescent sensor based on a lanthanide metal–organic framework. J Mater Chem A 5:5541–5549
51. Li Y, Yang M, Li P, Chen S, Li Y, Guo Z, Li S, Jiang M, Lin C, Huang X (2019) Changing the blood test: accurate determination of mercury (II) in one microliter of blood using oriented ZnO nanobelt array film solution-gated transistor chips. Small 15:1902433
52. Prabhu N, Chandra R, Rajendra B, George G, Mourad A, Shivamurthy B (2022) Electrospun ZnO nanofiber based resistive gas/vapor sensors -a review. Eng Sci 19:59–82. https://doi.org/10.30919/es8d612
53. Arun A, Malrautu P, Laha A, Ramakrishna S (2021) Gelatin nanofibers in drug delivery systems and tissue engineering. Eng Sci 16:71–81